The Sensitivity of the Tropical Hydrological Cycle to ENSO

B RIAN J. S ODEN

*National Oceanic and Atmospheric Administration/Geophysical Fluid Dynamics Laboratory,
Princeton, New Jersey*

ABSTRACT

Satellite observations of temperature, water vapor, precipitation and longwave radiation are used to characterize the variation of the tropical hydrologic and energy budgets associated with the El Niño–Southern Oscillation (ENSO). As the tropical oceans warm during an El Niño event, the precipitation intensity, water vapor mass, and temperature of the tropical atmosphere are observed to increase, reflecting a more vigorous hydrologic cycle. The enhanced latent heat release and resultant atmospheric warming lead to an increase in the emission of longwave radiation. Atmospheric global climate models, forced with observed sea surface temperatures (SSTs), accurately reproduce the observed tropospheric temperature, water vapor, and outgoing longwave radiation changes. However, the predicted variations in tropical-mean precipitation rate and surface longwave radiation are substantially smaller than observed. The comparison suggests that either (i) the sensitivity of the tropical hydrological cycle to ENSO-driven changes in SST is substantially underpredicted in existing climate models or (ii) that current satellite observations are inadequate to accurately monitor ENSO-related changes in the tropical-mean precipitation. Either conclusion has important implications for current efforts to monitor and predict changes in the intensity of the hydrological cycle.

1. Introduction

It has been suggested that warmer temperatures associated with increasing greenhouse gas emissions will increase precipitation intensity (via an increase in surface evaporation) and result in a more vigorous hydrologic cycle (IPCC 1996, p. 7 and references therein). Given the potential social, environmental, and economic consequences of such a scenario, developing a better understanding of the mechanisms that force changes in the hydrologic cycle and assessing the current skill of climate models in predicting such changes are of obvious importance. Climate variability associated with ENSO provides coherent changes in surface temperature and hydrologic variables that, while not necessarily a surrogate for global warming (Lau et al. 1996), does serve as a useful test bed for assessing the coupling between various components of the hydrologic cycle and for evaluating climate model performance. While considerable effort has been devoted to describing the regional changes in precipitation associated with ENSO, less attention has been given to characterizing variations in precipitation for the Tropics as a whole. Consequently, the skill of existing climate models in reproducing

natural variations in precipitation intensity over the Tropics and its coupling to other components of the hydrologic and energy budgets is not well known although its importance is clearly recognized (Chahine 1997).

To address this issue, satellite observations of precipitation, water vapor, tropospheric temperature, and outgoing longwave radiation are compared with simulations from a set of 30 different general circulation models (GCMs). All GCMs were integrated with observed sea surface temperatures (SSTs) for the period 1979–88 as part of the Atmospheric Modeling Intercomparison Project [AMIP; see Gates (1992) for details]. This period includes two warm "El Niño" events (1982–83, 1987–88) and two cold "La Niña" events (1984–85, 1988). Changes in the hydrologic cycle associated with ENSO are evaluated using satellite observations of precipitation from the microwave sounding unit (MSU; Spencer 1993) and from the Special Sensor Microwave Imager (SSM/I) as retrieved by Ferraro et al. (1996) and Wentz and Spencer (1998). Measurements of column-integrated water vapor are taken from the Scanning Multichannel Microwave Radiometer (SMMR; Wentz and Francis 1992) and the SSM/I (Wentz 1997). Observations of atmospheric temperature are obtained from the MSU (Spencer and Christy 1990) as well as from radiosonde analyses (Oort 1983); and outgoing longwave radiation measurements are acquired from the Earth Radiation Budget Experiment (ERBE;

Corresponding author address: Dr. Brian J. Soden, NOAA/Geophysical Fluid Dynamics Laboratory, P.O. Box 308, Princeton, NJ 08542.
E-mail: bjs@gfdl.gov

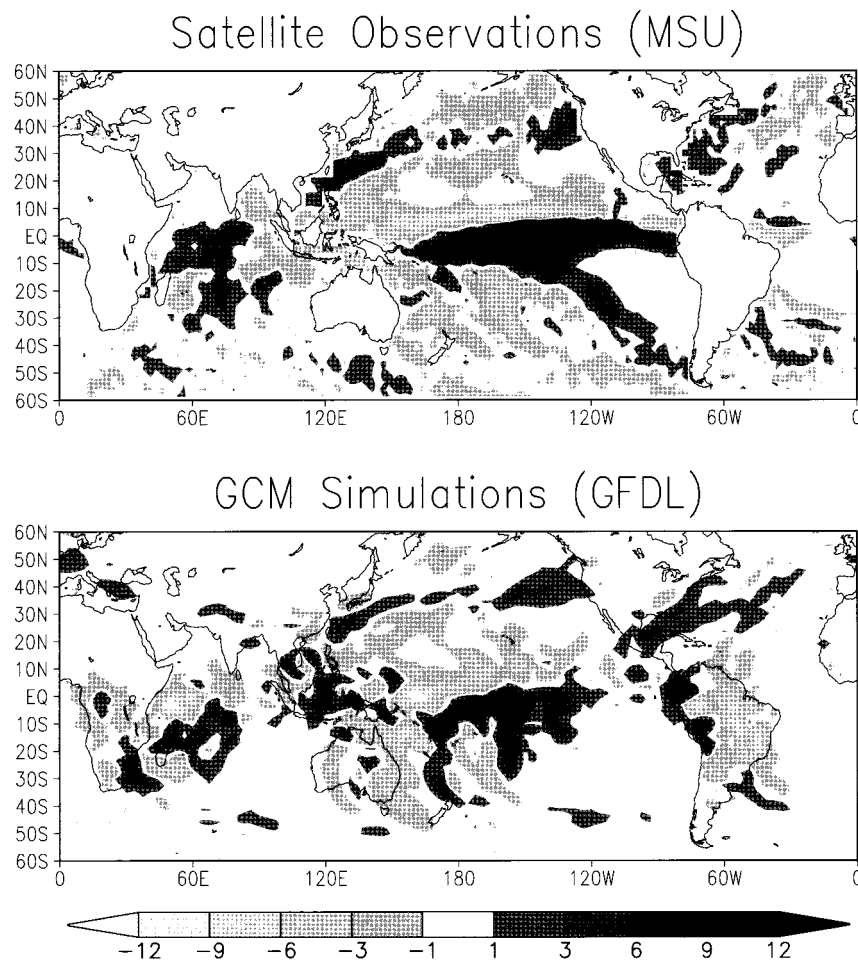## Satellite Observations (MSU)

GCM Simulations (GFDL)

FIG. 1. Map of the interannual difference in precipitation rate for a warm (El Niño) period minus a cold (La Niña) period. The difference corresponds to DJF 1982/83 minus DJF 1984/85 for (a) MSU observations and (b) AMIP simulations from the GFDL GCM.

Barkstrom 1984). These observations vary in length; however, all provide overlap with some portion of the AMIP study and thus provide an assortment of perspectives from which one can assess the skill of GCMs in simulating ENSO-related variations in the hydrological cycle.

2. Observed variations in the tropical hydrological cycle during ENSO

It is widely recognized that ENSO is associated with large regional changes in precipitation. These changes and their seasonal dependence have been extensively documented in many previous studies (e.g., Kiladis and Diaz 1989; Rasmusson and Arkin 1993; Ropelewski and Halpert 1996; Smith and Ropelewski 1997). Figure 1 shows the difference in P between a warm phase ([December–February (DJF)] 1982/83) and a cold phase (DJF 1984/85) from MSU observations (Fig. 1a) and AMIP GCM simulations (Fig. 1b). The GCM simulations are from a model developed at the Geophysical

Fluid Dynamics Laboratory (GFDL; Wetherald et al. 1991). Note that MSU precipitation retrievals are not performed over land. Such comparisons are useful for evaluating a model's skill in reproducing regional changes in precipitation associated with ENSO and are of great importance in their own right (e.g., Smith and Ropelewski 1997). However, they are less suitable for assessing the model's skill in predicting changes in the *intensity* of the hydrological cycle. This is because the precipitation variations at the regional scale (order of 1000 km) primarily reflect altered patterns of moisture transport rather than local changes in evaporation (Trenberth 1998). Consequently, the patterns of precipitation change in Fig. 1 are largely determined by changes in the large-scale atmospheric circulation and, hence, provide little insight into how the net precipitation for the Tropics as a whole is affected by ENSO. A better measure of the sensitivity of the tropical hydrologic cycle to ENSO may be obtained by considering the response of the tropical-mean precipitation rate. To reduce the effects of variations in moisture transport on the pre-
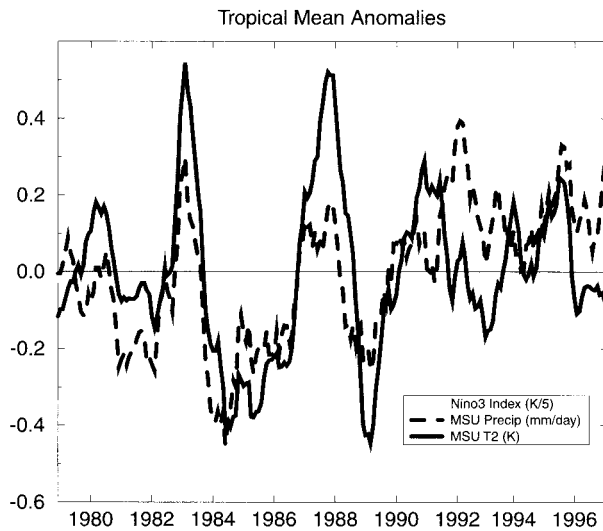
Tropical Mean Anomalies

FIG. 2. Time series of the tropical-mean interannual variations in MSU precipitation $\langle \delta P \rangle$ (dashed line), MSU channel-2 tropospheric temperature $\langle \delta P2 \rangle$ (thick solid line), radiosonde-weighted channel-2 temperature $\langle \delta T2_{\text{raob}} \rangle$ (thin solid line), and the Niño-3 SST index (shaded). All interannual anomalies are computed with respect to a base period of 1979–88. For clarity, all values have been smoothed using a 5-month running mean.

cipitation, this study examines variations in tropical-mean precipitation. Averaging over the entire Tropics (defined here as 30°N–30°S and spanning all longitudes) serves to reduce the effects of moisture transport that dominate the smaller-scale spatial variations (order of 1000 km; Trenberth 1998). Tropical averages were chosen over global averages due to the weakening of the ENSO signal in the global averages of all fields, the greater uncertainty in satellite precipitation measurements over extratropical regions, and the lack of water vapor and precipitation retrievals over land and ice-covered surfaces. While we recognize that the Tropics is not a closed system and that meridional transport of moisture form the Tropics does occur (e.g., monsoonal systems), the conclusions presented here are insensitive to this restriction. Repeating the analysis for averages between 60°N and 60°S leads to similar conclusions regarding the sensitivity of the observed and model-simulated hydrologic cycles, indicating that the they are not dependent upon the domain size chosen.

Figure 2 shows the interannual variation in tropical-mean precipitation rate from MSU (dashed line). This quantity is denoted as $\langle \delta P \rangle$, where δ represents the deviation from the seasonal climatology and "$\langle \, \rangle$" represents a spatially weighted average over the Tropics. For reference the Niño-3 SST index, defined as the SST anomaly averaged from 5°N to 5°S, and 90°W to 150°W, is also shown. Higher than normal surface temperatures in the tropical Pacific coincide with an increase in tropical-mean precipitation and thus a more vigorous hydrological cycle during an El Niño. Note that the variations in tropical-mean precipitation are substantially

smaller than the typical regional variations shown in Fig. 1. Consequently, the tropical-mean precipitation changes are of secondary importance to the regional variations in explaining precipitation variability at any particular location. Therefore, the relevance of examining tropical-mean variations is not for their role in determining local changes (which are largely transport dominated) but in examining how the intensity of the tropical-mean hydrological cycle responds to changing SSTs during ENSO. Although a trend toward positive precipitation anomalies appears in the data, it is not considered to be reliable. Recent analyses of MSU and SSM/I measurements (Spencer and Robertson 1998, personal communication) suggest that the MSU precipitation may be biased high after 1991 (although the cause of this potential bias is not known; see section 5 for more discussion of possible errors in the precipitation data).

Several earlier studies have also suggested that ENSO modulates the intensity of the tropical hydrological cycle (see Graham 1995). Radiosonde measurements reveal a strong correlation between interannual variations in tropospheric temperature and SSTs in the equatorial Pacific (Newell and Weare 1976; Pan and Oort 1990; Angell 1990). The atmospheric warming is widely considered to result from an intensified tropical hydrologic cycle during an El Niño. Observations indicate that during an El Niño elevated SSTs in the tropical Pacific increase the rate of evaporation (Flohn and Kappala 1989) and, consequently, the rate of precipitation also increases. It is believed that the resulting latent heat release warms the tropical atmosphere (Yulaeva and Wallace 1994) and produces the observed coupling between tropical Pacific SSTs and tropical atmospheric temperature.

MSU measurements of tropospheric temperature and precipitation are consistent with this picture. Figure 2 (solid line) shows the tropical-mean interannual variations in temperature from MSU channel 2 $\langle \delta T2 \rangle$, which measures the temperature over a deep layer of the troposphere atmosphere (roughly 1000–2000 hPa; Spencer and Christy 1990). Note the close correlation between Niño-3 SST, $\langle \delta P \rangle$, and $\langle \delta T2 \rangle$, indicating that enhanced SSTs in the tropical Pacific are associated with an increase in tropical-mean precipitation that, in turn, coincides with a warming of the tropical atmosphere. While previous studies have suggested that precipitation-driven latent heat fluxes link Niño-3 SSTs to the atmospheric temperature variations, there have been few (if any) attempts to directly verify this from observations.

Recent studies also suggest that the warming trend in global tropospheric temperature since the mid-1970s is linked to an enhancement of the tropical hydrological cycle (Angell 1990; Flohn et al. 1990; Graham 1995; Morrissey and Graham 1996; Diaz and Graham 1996). Graham (1995) demonstrated that when forced with observed SSTs the University of Hamburg ECHAM2
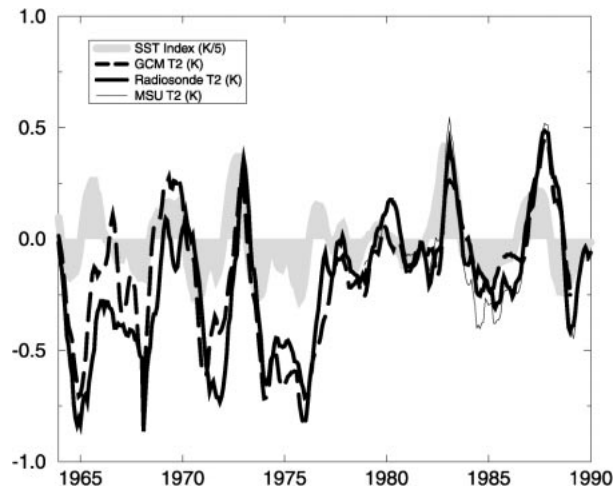
FIG. 3. Time series of the tropical-mean interannual variations in MSU channel-2 tropospheric temperature $\langle \delta T \rangle$ for 1979–89 (thin solid line), radiosonde-weighted channel-2 temperature $\langle \delta T2_{raob} \rangle$ for 1964–89 (thick solid line), GCM-weighted channel-2 temperature $\langle \delta T2_{raob} \rangle$ for 1964–88 (thick solid line), and the Niño-3 SST index (shaded). For clarity, all values have been smoothed using a 5-month running mean.

GCM accurately reproduces observed trends in global-mean surface air temperature. The upward trend in model-simulated temperature is caused by an enhancement of the hydrological cycle due to increasing SSTs. Thus the agreement between the observed and model-simulated temperature variations provided evidence that (indirectly) supported the model's skill in predicting changes in the hydrological cycle intensity. Comparisons between observed and model-predicted changes of tropical freezing heights (Diaz and Graham 1996) and precipitation trends over the tropical Pacific (Morrissey and Graham 1996) provide further evidence of this conclusion.

Figure 3 compares the observed variations in MSU $\langle \delta T2 \rangle$ (thin solid line) with that predicted from a version of the GFDL GCM $\langle \delta T2_{GCM} \rangle$ (thick dashed line) that has been integrated with observed SSTs for the period 1946–88 and from Oort's radiosonde analysis $\langle \delta T2_{raob} \rangle$ (thick solid line) for the period of 1964–89. Temperature and humidity profiles from both the GCM and radiosonde observations were inserted into a radiative transfer model (Eyre 1991) to compute the corresponding MSU channel-2 brightness temperature. Note that despite its poorer spatial coverage, the radiosonde analysis accurately captures variations in tropical-mean tropospheric temperature measured by MSU and can therefore be used to extend the observational record back to 1964. When evaluated over this longer time period, the GCM closely reproduces the observed variations in tropospheric temperature (with the exception of earlier parts of the radiosonde record). The question that remains, however, is to what extent this indirect comparison provides evidence of the model's ability to simulate changes in the intensity of the tropical hydrological cy-

cle. This question, which has also been raised previously (Diaz and Graham 1996; Morrissey and Graham 1996), is addressed in the next two sections by comparing the observed relationships between precipitation, water vapor, temperature, and outgoing longwave radiation to that predicted by a set of 30 different GCMs.

3. Comparison of observed variations with AMIP simulations

a. Precipitation rate

To evaluate the sensitivity of the tropical hydrological cycle to ENSO, the observed changes in tropical-mean precipitation are compared with that predicted by the AMIP set of GCM simulations. Figure 4a shows the time series of MSU observed $\langle \delta P \rangle$ from 1979 to 1996 (thick line). Also shown is the multimodel ensemble-mean value of $\langle \delta P \rangle$ (thin line) from the 30 different GCMs that participated in AMIP (Table 1). To be consistent, both the MSU-observed and GCM-simulated interannual variations are computed with respect to a common base period of 1979–88. Since the observations are restricted to ocean surfaces, the model $\langle \delta P \rangle$ is also averaged only from oceanic grids to provide comparable quantities. The multimodel ensemble-mean $\langle \delta P \rangle$ is computed by averaging all models for that particular month, and the range bounded by $\pm$ one intermodel standard deviation in $\langle \delta P \rangle$ is shown as a vertical bar. Further analysis of the intermodel variability is described in section 4b.

The chief feature in this plot is the substantial difference between the observed and GCM-simulated variation in tropical-mean precipitation. While the precipitation rate in both the observations and model simulations tends to increase with SST, the magnitude of the observed variations in $\langle \delta P \rangle$ is substantially larger than that predicted by current GCMs and clearly lies outside the range of intermodel variability. Also note that the intermodel variability in $\langle \delta P \rangle$ is nearly as large as the ensemble-mean ENSO signal. Thus, not only do the GCMs differ with respect to the observations, but the models also lack coherence among themselves. It is noted, however, hat even the extreme models exhibit markedly less precipitation variability than observed. For example, the monthly standard deviation of $\langle \delta P \rangle$ (denoted as $\sigma \langle \delta P \rangle$) computed separately for each of the 30 GCMs ranges from 0.03 to 0.10 mm day^{-1}, with an average value of 0.06 mm day^{-1}. In comparison, $\sigma \langle \delta P \rangle$ from MSU for the period 1979–88 is 0.18 mm day^{-1}. For typical tropical-mean precipitation rates (~ 3 mm day^{-1}), the observations suggest relative fluctuations of roughly $\pm 6\%$, whereas the models typically yield about one-third this value. If the observations are correct, this would indicate that the sensitivity of the tropical-mean hydrological cycle to ENSO-driven SST changes is substantially underpredicted in current models. Moreover, the diversity of models considered here requires that
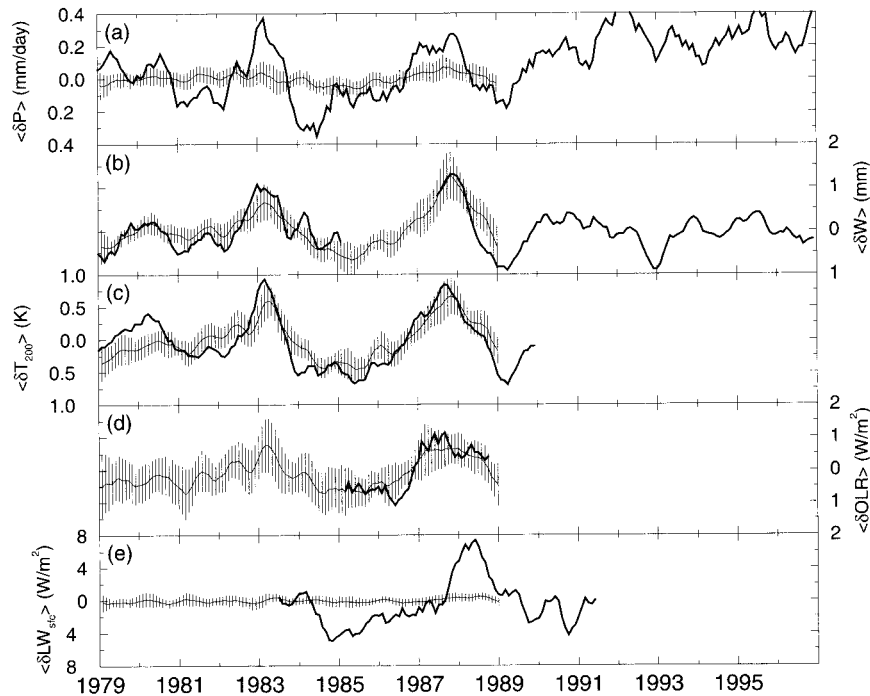
FIG. 4. Time series of the tropical-mean interannual variations of observations (thick solid line) and multimodel ensemble-mean of AMIP GCM simulations (thin solid line) for (a) precipitation rate, (b) total precipitable water vapor, (c) 200-hPa atmospheric temperature, (d) OLR, and (e) net surface longwave radiation. The range bounded by $\pm$ one intermodel standard deviation is represented by the vertical lines centered on the multimodel ensemble-mean GCM value. See text for details. For clarity, both the observed and GCM-simulated time series have been smoothed using a 5-month running mean. Typical values of the tropical-mean (total) observed fields are: $\langle P \rangle \cong 3$ mm day^{-1}, $\langle W \rangle \cong 38$ mm, $\langle T_{200} \rangle \cong 220$ K, $\langle$OLR$\rangle \cong 250$ W m^{-2}, $\langle$LW$_{\text{sfc}}\rangle \cong -50$ W m^{-2}.

this error not be sensitive to the differing physical parameterizations between existing GCMs. Rather, if the GCMs are in error, this deficiency would presumably reflect a more fundamental flaw common to all models.

An alternative explanation is that the MSU precipitation observations contain a systematic error that is correlated with ENSO. Of particular concern is the potential for interannual variations in tropospheric temperature to influence the microwave emission signal and thereby bias the precipitation estimate. While the potential for such an error is known to exist, its magnitude is not (e.g., Spencer et al. 1998). Indeed, the sensitivity of the passive microwave precipitation retrievals to temperature variations is not well known and clearly requires further attention. A definitive resolution of this issue will obviously require a detailed analysis of various microwave-based rainfall algorithms to determine their temperature sensitivity. While such an analysis is beyond the scope of the present study, this study does provide some evaluation of the MSU product by comparing variations $\langle \delta P \rangle$ from MSU with that obtained from various SSM/I retrievals (section 5). While this certainly does not represent a "ground-truth" validation of the MSU product, it does provide some indication of how it compares to other retrievals.

b. Water vapor

It is useful to examine the model simulations of other components of the tropical hydrologic and energy budgets, to determine if they also exhibit discrepancies with the observations. Figure 4b presents a time series of the interannual variations in tropical-mean precipitable water $\langle \delta W \rangle$ derived from SMMR for 1979–84 and SSM/I for July 1987–1996. The local (rms) errors in SSM/I retrievals of W are estimated to be $\sim$1.2 mm, with time-mean biases of $\sim$0.6 mm (Wentz 1997). Also shown is the multimodel ensemble-mean and intermodel standard deviation of $\langle \delta W \rangle$ from the AMIP GCM simulations. For consistency, the interannual variations in SMMR observations and GCM simulations are computed with respect to a base period of 1979–84. The SSM/I observations provide only 18 months of overlap with the GCM simulations (July 1987–December 1988) and therefore use a different base period (1988–96) for computing the interannual variability. Both the observations and model predictions clearly show that the total atmospheric water vapor mass increases during the warm events (1982–83, 1987–88) and decreases during the cold events (1984–85, 1988–89). In contrast to the precipitation variations, the GCMs exhibit good agreement

TABLE 1. List of AMIP models.

No.	Acronym	AMIP group	Resolution
1	BMRC	Bureau of Meteorology Research Centre	R31 L9
2	CCC	Canadian Centre for Climate Modelling and Analysis	T32 L10
3	CNRM	Centre National de Recherches Météorologique	T42 L20
4	CSU	Colorado State University	4×5 L17
5	DERF	Dynamical Extended Range Forecasting (at GFDL)	T42 L18
6	ECMWF	European Centre for Medium-Range Weather Forecasts	T42 L19
7	GFDL	Geophysical Fluid Dynamics Laboratory	R30 L14
8	GISS	Goddard Institute for Space Studies	4×5 L9
9	GLA	Goddard Laboratory for Atmospheres	4×5 L17
10	GSFC	Goddard Space Flight Center	4×5 L20
11	IAP	Institute of Atmospheric Physics	4×4 L2
12	JMA	Japan Meteorological Agency	T42 L21
13	MGO	Main Geophysical Observatory	T30 L14
14	MPI	Max-Planck Institut für Meteorologie	T42 L19
15	MRI	Meteorological Research Institute	4×5 L19
16	NCAR	National Center for Atmospheric Research	T42 L18
17	NMC	National Meteorological Center	T40 L18
18	NRL	Naval Research Laboratory	T47 L18
19	SUNYA/NCAR	State University of New York at Albany/National Center for Atmospheric Research	T31 L18
20	UCLA	University of California, Los Angeles	4×5 L15
21	UGAMP	U.K. Global Atmospheric Modelling Programme	T42 L19
22	UIUC	University of Illinois at Urbana–Champaign	4×5 L7
23	YONU	Yonsei University	4×5 L5
24	COLA	Center for Ocean–Land–Atmospheric Studies	R40 L18
25	CSIRO	Commonwealth Scientific and Industrial Research Organization	R21 L9
26	DNM	Department of Numerical Mathematics	4×5 L7
27	LMD	Laboratoire de Météorologie Dynamique	3.6×5.6 L11
28	SUNYA	State University of New York at Albany	R15 L12
29	UKMO	United Kingdom Meteorological Office	2.5×3.75 L19
30	CCSR	Center for Climate System Research	T21 L20

with both the magnitude and sign of the observed changes in water vapor. This result is significant for two reasons. First, it demonstrates the models' ability to predict SST-driven changes in tropical-mean water vapor, which is an important aspect of GCMs climate simulations that had been previously questioned (Sun and Held 1996; Chou 1994). Second, it indicates that the residual between evaporation and precipitation, namely, the change in water vapor storage by the atmosphere, is well represented in the GCMs. Thus, if ENSO-driven changes in tropical-mean precipitation are being systematically underestimated in GCMs, this deficiency is not attributable to errors in the simulated water vapor field (e.g., not enough water vapor to condense).

c. Atmospheric temperature

The interannual changes of the latent heat release from precipitation may be estimated by scaling $\langle \delta P \rangle$ by 28.9 W m^{-2} (mm day^{-1}). Accordingly, the observed $\langle \delta P \rangle$ implies changes in tropical-mean latent heating of roughly ± 6 W m^{-2} between warm and cold ENSO events, whereas the typical model-simulated changes are roughly a factor of 4 smaller. Since changes in latent heat release are a primary source of energy for warming the atmosphere during El Niño (Graham 1995), one might expect that systematic differences in tropical-mean precipitation would result in differences in tro-

pospheric temperature variations. Figure 4c compares the interannual variations in tropical-mean temperature at 200 hPa $\langle \delta T_{200} \rangle$ determined from radiosonde analyses (Oort 1983) to the GCM simulations. Both the observed and model-simulated interannual variability are computed with respect to a common base period (1979–88). Radiosonde analyses are used rather than MSU temperature measurements because AMIP archived temperatures only at 200 and 850 hPa. Hence, reconstruction of the deep-layer mean temperatures for comparison with MSU is not possible. As expected, the observed variations in tropical-mean temperature $\langle \delta T_{200} \rangle$ are closely reproduced by the GCMs. Given the close coupling between changes in latent heat release (i.e., precipitation) and atmospheric temperature suggested by earlier studies and from the GCM, it is natural to cite this agreement as evidence of the skill of the GCM in predicting changes in the hydrologic cycle intensity (e.g., Graham 1995). Indeed, the extent of agreement between the observed and modeled temperature variations is quite surprising given the magnitude of their differences in $\langle \delta P \rangle$. This would suggest that either the observed variations in $\langle \delta P \rangle$ are incorrect (which is discussed further in section 5) or that there is some other systematic error in the GCM energy budgets that compensates for the difference in latent heat release. Given that the GCMs considered here differ significantly in their physical parameterization, the source of model er-

ror would not only have to be insensitive to details of the model physics but, more importantly, be consistently manifest in all the GCMs.

d. Radiation

Over the Tropics, the latent heat released from tropical precipitation is largely offset by radiative cooling due to the emission of outgoing longwave radiation (OLR) to space (Pierrehumbert 1995). Consequently, the atmospheric temperature change is primarily determined by the residual between changes in latent heat release and OLR (Graham 1995). Thus it is conceivable that a model could underpredict the increase in tropical-mean precipitation during an El Niño, yet accurately simulate the atmospheric warming if the increase in model-simulated radiative cooling was also underpredicted. That is, mutually consistent errors in the ENSO-driven changes of latent heating (i.e., precipitation) and radiative cooling (i.e., OLR) of the models could conceivably offset each other in such a way as to produce a realistic temperature change.

To investigate this possibility, the observed interannual variation in tropical-mean outgoing longwave radiation $\langle \delta \text{OLR} \rangle$ from ERBE is compared to that obtained from the AMIP GCM simulations for the period 1985–88 (Fig. 4d). To eliminate the effects of calibration differences between satellite instruments (Thomas et al. 1995), only observations from one satellite (*ERBS*) are considered here. As with $\langle \delta W \rangle$ and $\langle \delta T_{200} \rangle$, the observed variations in $\langle \delta \text{OLR} \rangle$ exhibit relatively good agreement with the AMIP GCM simulations, suggesting that errors in the infrared radiative cooling do not explain the current discrepancy.

In addition to OLR, the other term in the longwave radiative cooling budget is the net flux of downwelling radiation at the surface, LW_{sfc} (Graham 1995). While retrieval of LW_{sfc} from satellite observations is difficult at best, some attempts have been made. Figure 4e compares the observations of $\langle \delta \text{LW}_{sfc} \rangle$ from the dataset of Darnell et al. (1996) with that predicted from the 30 GCMs. Interestingly, the observed variations are substantially larger than simulated by the models. The sign is such that the GCMs tend to underestimate (overestimate) the anomalies in radiative heat lost from the atmosphere to the surface during a warm (cold) ENSO event by about 5 W m^{-2}. Thus both the magnitude and sign of the LW_{sfc} anomalies are, to first order, consistent with the discrepancy between the observed and GCM-simulated precipitation anomalies. However, given the considerable uncertainty involved in retrieval of LW_{sfc}, it is not clear if this is simply a coincidence or if it is a true manifestation of systematic errors in the GCMs' hydrologic and energy budgets.

Other components of the energy budget that are difficult to observe, but whose variations are considered to be of secondary importance (Graham 1995), are sensible heat flux and the absorption of solar radiation. The latter quantity is one in which there has been considerable debate regarding the accuracy of its representation in current GCMs, particularly the absorption of solar radiation by clouds (Cess et al. 1996). While this mechanism could provide a systematic source of error in all models, it is unclear whether the error would be of the correct sign, let alone the correct magnitude, to explain the discrepancy presented here. Compensating for the discrepancies between observed and model-simulated latent heating (inferred from $\langle \delta P \rangle$) would require interannually varying errors in tropical-mean solar absorption of ~4–5 W m^{-2}.

4. Relationship with sea surface temperature

a. Ensemble-mean results

To help quantify the differences between the observations and models, Fig. 5 shows a scatterplot of $\langle \delta P \rangle$, $\langle \delta W \rangle$, $\langle \delta T_{200} \rangle$, and $\langle \delta \text{OLR} \rangle$ versus the corresponding value of $\langle \delta \text{SST} \rangle$ for both the observations (open circles) and the multimodel ensemble-mean of the AMIP GCM simulations (filled circles). Pearson correlation coefficients (r) and least squares linear regression slopes (s) are listed in Fig. 5. For each quantity, the scatterplot is constructed from only those months for which both observations and AMIP simulations are available, ensuring a consistent sampling of the two quantities. For both the observations and models, all four quantities (P, W, T_{200}, and OLR) are well correlated with SST. The correlations in the GCMs for all quantities are systematically larger than those from the observations, since ensemble averaging of the GCM results reduces the climate "noise." For W, T_{200}, and OLR, the rate of increase with increasing SST predicted by the models agrees well with the observed values. However, for tropical-mean precipitation, the observed rate of increase with SST is roughly a factor of 4 larger than predicted by the GCMs. Interestingly, the slopes for the GCM simulations of W, T_{200}, and OLR all tend to be ~20% smaller than their observed counterpart. Whether or not this difference in slopes is meaningful is unclear; however, the fact that it shows up consistently in all three variables (W, OLR, T_{200}) is nonetheless intriguing.

b. Intermodel variability

The preceding results have largely focused on the ensemble-mean behavior of the 30 different GCMs. However, there is, of course, considerable variability from one model to the next. The above statements largely reflect the ensemble characteristics of the models, rather than a universal statement of all models. In addition to comparing the multimodel ensemble-mean GCM results with the observations, Fig. 4 also shows the magnitude of the intermodel variability relative to the amplitude of the tropical-mean variations for any particular month. A key feature here is that the intermodel variability in $\langle \delta P \rangle$ is
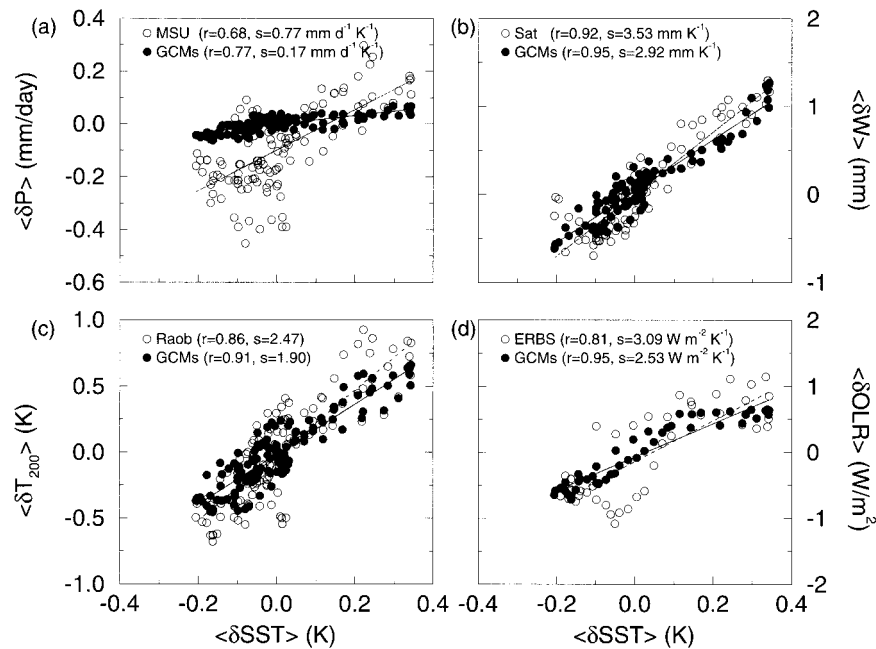
FIG. 5. Scatterplot of the tropical-mean interannual variations in (a) precipitation rate, (b) total precipitable water vapor, (c) atmospheric temperature, and (d) OLR as a function of the tropical-mean interannual variations in SST. Tropical averages of precipitation and precipitable water are from ocean regions only. Results are shown for both observations (open circles) and the ensemble-mean of the AMIP GCM simulations (filled circles). Linear correlation coefficients (r) and least squares regression slopes (s) for both the observations (dotted line) and models (solid line) are also shown. All values were smoothed using a 5-month running mean before computing the regression and correlation coefficients.

nearly as large as the ENSO signal in the ensemble-mean GCM simulations (but still smaller than the observed ENSO signal). On the other hand, for $\langle\delta W\rangle$, $\langle\delta T_{200}\rangle$, and to a slightly lesser extent $\langle\delta OLR\rangle$, the amplitude of the ENSO signal clearly stands out above the intermodel variability. This shows that not only is the multimodel ensemble-mean behavior of the GCMs in better agreement with the observations for the latter three quantities, but also that the GCMs are also in better agreement with each other in terms of the amplitude of the tropical-mean variation for any particular month.

To further highlight the intermodel variability, Fig. 6 compares the slope of the linear regression between the tropical-mean interannual variation of each of the four quantities versus $\langle\delta SST\rangle$. The slopes were computed separately for each of the 30 GCMs considered above (listed in Table 1) as well as for the observations. The dashed line represents the slope computed from the ensemble-mean of the 30 GCMs (i.e., the slopes shown in Fig. 5). To emphasize the lower-frequency variations and maintain consistency with Fig. 5, all values are smoothed using a 5-month running mean before computing the regression. Two points are to be made with this analysis. The first is that for a given increase in $\langle\delta SST\rangle$, the observed increase in $\langle\delta P\rangle$ is not only much larger than the ensemble mean of the GCMs (dashed line), but it also overshadows all of the models indi-

vidually. In contrast, the observed increases for $\langle\delta W\rangle$, $\langle\delta T_{200}\rangle$, and $\langle\delta OLR\rangle$, are much more consistent with the GCM predictions, clearly lying within the range of intermodel variability. This is perhaps most clearly illustrated by considering the number of GCMs for which the predicted slope falls within a factor of 2 of the observed slope. For $\langle\delta W\rangle$ this number is 28 out of 30 models, for $\langle\delta T_{200}\rangle$ it is 27/30, and for $\langle\delta OLR\rangle$ 21/30. However, for $\langle\delta P\rangle$ only 2 out of 30 GCMs fall within a factor of 2 of the observed slope.

The second point is that the GCM-simulated slopes for $\langle\delta P\rangle$ exhibit a wide range of values, indicating little consistency among the models. In contrast, the model-simulated slopes for $\langle\delta W\rangle$ and $\langle\delta T_{200}\rangle$ are in much better agreement with each other. Interestingly, there also tends to be a larger range of intermodel variability for $\langle\delta OLR\rangle$. This may be attributable to differences in the model predictions of cloud cover variations, which also influence the OLR. Furthermore, of the four variables examined, OLR has the shortest record of observations (only 4 yr). Thus the shorter time period for the analysis may also contribute to the greater intermodel variability.

5. Intercomparison of tropical-mean precipitation measurements

The other possible explanation for the discrepancy in $\langle\delta P\rangle$ is that the MSU retrieval is in error. This is of
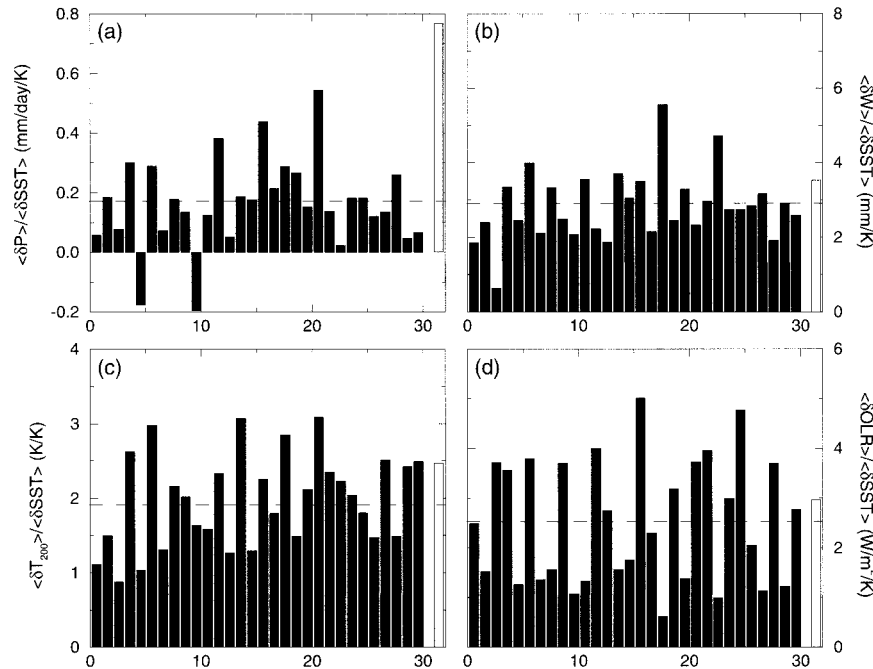
FIG. 6. Bar graph of the least squares regression slope of the tropical-mean interannual variations in (a) precipitation rate, (b) total precipitable water vapor, (c) 200-hPa atmospheric temperature, and (d) OLR as a function of the tropical-mean interannual variations in SST. Results are shown separately for all 30 GCMs listed in Table 1 (dark shading) and for the observations (light shading). The dashed line represents the slope computed from the multimodel ensemble mean of the 30 GCMs (i.e., the slopes shown in Fig. 5). To emphasize the lower-frequency variations, all values were smoothed using a 5-month running mean before computing the regression.

particular concern given the relatively small magnitude of $\langle \delta P \rangle$ and the inherent difficulty of accurately measuring precipitation. The most comprehensive evaluation of passive microwave satellite retrievals to date is the Precipitation Intercomparison Project 2 (PIP-2). Results from this project, which evaluated the performance of 20 different SSM/I algorithms, suggest bias uncertainties in retrieved precipitation of roughly ±30% for most algorithms (Smith et al. 1998). Note that this uncertainty was considered to be smaller than that of the radar and rain gauge data collected for validation. Since the amplitude of $\langle \delta P \rangle$ observed by MSU (Fig. 4) is roughly ±10%, it falls within the uncertainty range of PIP-2. However, it is important to note that PIP-2 compared retrievals at full-resolution instantaneous space–timescales. Since the error characteristics are likely to be scale dependent, point comparisons like PIP-2 may not necessarily provide appropriate estimates of the uncertainty in microwave-based retrievals of $\langle \delta P \rangle$. Sources of error that are dominant for point comparisons (e.g., subpixel variability) are not the same for tropical-mean anomalies. The latter average out spatially uncorrelated errors, but they are more susceptible to errors introduced by temperature or cloud liquid water variations that are locally small but that occur systematically throughout the Tropics in association with ENSO.

Unfortunately, there are no in situ measurements with sufficient spatial coverage to validate tropical-mean satellite measurements; therefore, the error characteristics of the satellite observations at these large spatial scales remain poorly understood. Since the enhanced sensitivity of $\langle \delta P \rangle$ is clearly associated with ENSO, the most likely source of error would come from contamination of the upwelling microwave radiance by ENSO-related changes in water vapor, cloud liquid water, and atmospheric or surface temperature that could bias the amplitude of the retrieved precipitation. However, this explanation remains speculative. The only other study to critically examine tropical-mean precipitation anomalies (Spencer et al. 1998) reached the same conclusion, that is, that uncertainties associated with aliasing temperature variations into the precipitation retrievals represent a potential, but currently unknown, source of error that requires further attention from the retrieval community.

Since ground-truth measurements are not available for $\langle \delta P \rangle$, one way of assessing the reliability of the MSU product is to intercompare its measurements with that obtained from other satellite retrievals. The SSM/I, which has been in operation since July 1987, contains better frequencies for rainfall retrieval and also provides the opportunity to intercompare rainfall measurements using different retrieval strategies. Figure 7 compares the tropical-mean interannual variation in precipitation from MSU (solid line) with that using the SSM/I re-
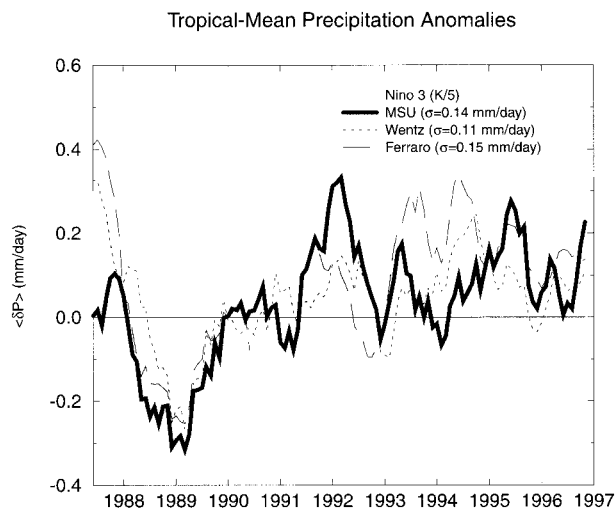
Tropical-Mean Precipitation Anomalies

FIG. 7. Comparison of the tropical-mean interannual variations in precipitation rate $\langle \delta P \rangle$ from various satellite measurements. The interannual anomalies are computed with respect to a base period of 1988–96. Consequently, the MSU $\langle \delta P \rangle$ differs slightly from that presented in Fig. 2 (which used a base period of 1979–88). For clarity, all values have been smoothed using a 5-month running mean.
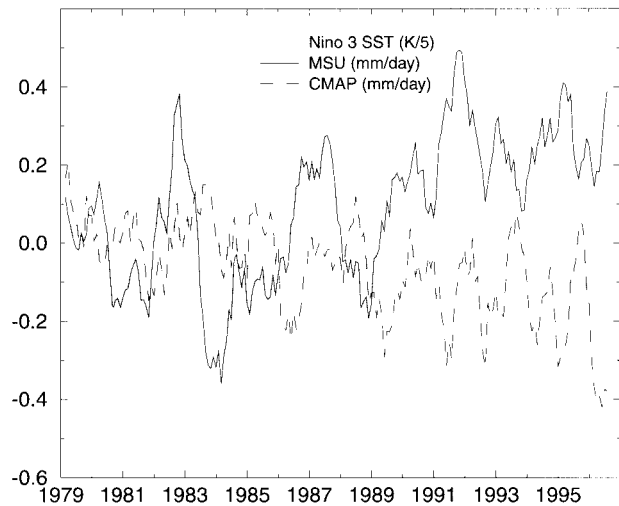

FIG. 8. Comparison of the tropical-mean interannual variations in precipitation rate $\langle \delta P \rangle$ from MSU and CMAP. The interannual anomalies are computed with respect to a base period of 1979–88. For clarity, all values have been smoothed using a 5-month running mean.

trievals of Wentz and Spencer (1998) (dotted line) and Ferraro et al. (1996) (dashed line). The Wentz and Spencer algorithm uses the emission signal in the 19-, 22-, and 37-GHz channels of SSM/I to estimate precipitation rates. The algorithm is designed to orthogonalize the retrievals so that "cross talk" between parameters such as water vapor and rainfall is minimized (i.e., errors in retrieved rain rate are uncorrelated with errors in retrieved water vapor). This algorithm also adjusts for the effects of air temperature and cloud liquid water on the microwave radiance. The Ferraro et al. (1996) algorithm is based upon the scattering signature of precipitation in the 85-GHz channel (Grody 1991) supplemented by the Weng and Grody (1994) emission technique over oceans. Due to the failure of the 85-GHz channels no retrievals are available from this algorithm during the period of July 1990–December 1991.

Comparison of the interannual variations between the SSM/I and MSU measurements (Fig. 7) reveals reasonably good agreement from 1988 to 1992; however, they diverge between mid-1992 and 1994. The lack of coherence between the retrievals during this period may partly reflect the impact of Mount Pinatubo aerosols on the precipitation retrievals (Spencer et al. 1998). It is also noteworthy that all retrievals show noticeably larger variations in $\langle \delta P \rangle$ than predicted by the GCMs. This is particularly evident for the 1988/89 La Niña where all three retrievals exhibit a marked reduction in $\langle \delta P \rangle$. Linear regression of $\langle \delta P \rangle$ versus $\langle \delta SST \rangle$ for the period of 1988–96 (not shown) yields slopes of 0.41 mm day^{-1} K^{-1} for MSU, 0.53 mm day^{-1} K^{-1} for the Wentz and Spencer algorithm, and 0.69 mm day^{-1} K^{-1} for the Ferraro algorithm. Note that the slopes differ by roughly ±25%, although there is no indication that the MSU

measurements overestimate the changes in $\langle \delta P \rangle$. Indeed for the period 1988–96, the MSU measurements tend to be slightly less sensitive to changes in SST than do either of the SSM/I retrievals considered here. Thus if the large variability in the MSU $\langle \delta P \rangle$ is erroneous, then this problem is apparently shared by other precipitation products that use different frequency channels and different retrieval algorithms. This suggests that simply attributing the discrepancy between observed and GCM-simulated variations in $\langle \delta P \rangle$ to observational error in the MSU product may be premature. It is also noted that Spencer and Robertson (1998, personal communication) find very good agreement between tropical-mean anomalies of precipitation from SSM/I and an MSU index of deep convection.

In choosing precipitation measurements for the above comparison, attention was restricted to products derived from a single instrument, rather than from datasets produced by merging several different measurement systems. An example of the latter is the Climate Prediction Center Merged Analysis of Precipitation (CMAP) product (Xie and Arkin 1997), which combines microwave and infrared measurements from multiple satellites with surface gauge measurements and model analyses. While this product has several advantages over single-measurement climatologies like MSU, one potential limitation is that temporal discontinuities in the availability or sampling of individual data sources can hinder the ability to detect the small, time-dependent anomalies of $\langle \delta P \rangle$. Figure 8 compares time series of $\langle \delta P \rangle$ from both MSU and CMAP (averaged only from oceanic regions). Note that both the CMAP and MSU measurements show much larger variations in $\langle \delta P \rangle$ than do the GCMs. However, even though CMAP uses MSU in its composite product, the time series of $\langle \delta P \rangle$ are substantially dif-

ferent. Interestingly, the CMAP measurements exhibit little correlation with changes in SST, in contrast to both MSU observations and most models. The cause of this difference is unclear and obviously indicates a problem in either the MSU or CMAP products (or both). The comparison also underscores the discrepancies that exist between the current precipitation climatologies and the challenge of accurately monitoring changes in the intensity of the hydrological cycle.

6. Discussion

Satellite observations of the ENSO-driven changes in tropical-mean precipitation, water vapor, temperature, and outgoing longwave radiation were compared with simulations from a set of 30 different GCMs. In both observations and GCM simulations, the precipitation increases during a warm phase of ENSO; however, the magnitude of the model-predicted change is roughly a factor of 4 smaller than observed. In contrast, the model-simulated changes in tropical-mean water vapor, atmospheric temperature, and outgoing longwave radiation all demonstrate very good agreement with the observations. Given the close coupling that these quantities have to the hydrologic and energy budgets, this evidence would seem to support of the models' skill in simulating changes in hydrological cycle intensity (Graham 1995). However, the extent to which the comparison of $\langle \delta T_{200} \rangle$ (and similarly $\langle \delta W \rangle$, $\langle \delta \text{OLR} \rangle$) provides a test of the models' skill in predicting changes in hydrological cycle intensity is not entirely clear. For example, one can view the tropical climate from the perspective of an atmosphere in radiative–convective equilibrium. Such an atmosphere responds to surface temperature perturbations by restoring the atmospheric temperature profile to closely follow a moist-adiabatic lapse rate. Thus, when examining temperature changes predicted by a GCM forced with observed SSTs, one is therefore faced with the following dilemma: is the atmospheric temperature determined by the *balance of radiative and latent energy fluxes predicted by the model,* or is the balance of radiative and latent energy fluxes in the model *determined by the atmospheric temperature* (i.e., the need for the atmosphere to follow a moist adiabat)? For example, if a GCM (forced with observed SSTs) did contain a systematic error in one term of the energy budget (e.g., surface radiative cooling), would the impact of this error be manifest in the GCM's temperature field or would the model still adjust to a moist adiabat, thereby forcing a compensating error in some other term of the energy budget (e.g., latent heat flux)?

These questions are posed mainly to suggest that agreement between observed and GCM-simulated $\langle \delta T_{200} \rangle$, $\langle \delta W \rangle$, and $\langle \delta \text{OLR} \rangle$, while informative in its own right, may not necessarily provide enough evidence to dismiss the possibility of errors in the GCM-simulated $\langle \delta P \rangle$. Nevertheless, the inherent coupling of the hydrologic and energy budgets does place some constraints on this analysis. It suggests that if the variability in tropical-mean precipitation is being underestimated in current GCMs, then there must also be a compensating error in the tropical energy budget in order for the models to reproduce the agreement with observed air temperature variations. Furthermore, given the prevalence of this discrepancy, the source of error would presumably be common to all GCMs. That is, the deficiency would not be attributable to a particular physical parameterization or model resolution, but rather would result from a more fundamental error that occurs in all GCMs. The possibility that the errors in GCM-simulated $\langle \delta P \rangle$ may be associated with errors in $\langle \delta \text{LW}_{\text{sfc}} \rangle$ (see Fig. 4) is intriguing and illustrates the intrinsic coupling between the energy and the hydrologic budgets. If true, the cause of such an error might be related to boundary layer clouds, which exhert a strong influence over the LW_{sfc} and are known to be poorly represented in many GCMs.

The other possible explanation is that the satellite retrievals systematically overestimate the amplitude of the interannual variability in tropical-mean precipitation and the net LW cooling of the surface. A primary difficulty in identifying the cause of the discrepancy between observed and model-simulated $\langle \delta P \rangle$ (and $\langle \delta \text{LW}_{\text{sfc}} \rangle$) stems from a lack of knowledge of the error characteristics in the retrievals at these spacescales and timescales. While measurements from different sensors and different algorithms tend to support the magnitude of the MSU-retrieved $\langle \delta P \rangle$ (e.g., Spencer and Robertson 1998, personal communication), further work is necessary to better define this aspect of the precipitation products. If the observations are incorrect, it would suggest that current observations are inadequate to accurately describe changes in the intensity of the tropical hydrologic cycle.

Clearly, considerable progress is required before we can have confidence in our ability to both monitor *and* predict changes in the intensity of the hydrologic cycle. Given the possibility of future changes associated with global warming, this issue certainly warrants further attention.

REFERENCES

Angell, J. K., 1990: Variation in global tropospheric temperature after adjustment for the EL Niño influence, 1958–1989. *Geophys. Res. Lett.,* **17,** 1093–1096.

Barkstrom, B. R., 1984: The Earth Radiation Budget Experiment (ERBE). *Bull. Amer. Meteor. Soc.,* **65,** 1170–1185.

Cess, R. D., M. H. Zhang, Y. Zhou, and V. Dvortsov, 1996: Absorption of solar radiation by clouds: Interpretation of satellite, surface

and aircraft measurements. *J. Geophys. Res.,* **101,** 23 299–23 309.

Chahine, M., 1997: Accelerating the hydrological cycle. *GEWEX News,* May.

Chou, M. D., 1994: Coolness in the tropical Pacific during an El Niño episode. *J. Climate,* **7,** 1684–1692.

Darnell, W. L., W. F. Staylor, N. A. Ritchey, S. K. Gupta, and A. C. Wilber, 1996: Surface radiation budget: A long-term global dataset of shortwave and longwave fluxes. [Available online at http://www.agu.org/eos_elec/95206e.html.]

Diaz, H. F., and N. E. Graham, 1996: Recent changes in tropical freezing heights and the role of sea surface temperatures. *Nature,* **383,** 152–155.

Eyre, J. R., 1991: A fast radiative transfer model for satellite sounding systems. ECMWF Tech. Memo. 176, 28 pp.

Ferraro, R., F. Weng, N. Grody, and A. Basist, 1996: An eight-year (1987–1994) time series of rainfall, clouds, water vapor, snow cover, and sea ice derived from SSM/I measurements. *Bull. Amer. Meteor. Soc.,* **77,** 891–905.

Flohn, H., and A. Kappala, 1989: Changes of tropical sea–air interaction processes over a 30-year period. *Nature,* **262,** 244–266.

——, ——, H. Knoche, and H. Mächel, 1990: Recent changes of the tropical water and energy budget and of midlatitude circulations. *Climate Dyn.,* **4,** 237–252.

Gates, W. L., 1992: AMIP: The Atmospheric Model Intercomparison Project. *Bull. Amer. Meteor. Soc.,* **73,** 1962–1970.

Graham, N. E., 1995: Simulation of recent global temperature trends. *Science,* **267,** 666–671.

Grody, N. C., 1991: Classification of snow cover and precipitation using the Special Sensor Microwave/Imager. *J. Geophys. Res.,* **96,** 7423–7435.

IPCC, 1996: *Climate Change 1995: The Science of Climate Change.* Cambridge University Press, 572 pp.

Kiladis, G., and H. Diaz, 1989: Global climatic anomalies associated with extremes in the Southern Oscillation. *J. Climate,* **2,** 1069–1090.

Lau, K. M., C. H. Ho, and M. D. Chou, 1996: Water vapor and cloud feedback over the tropical oceans: Can we use ENSO as a surrogate for climate change? *Geophys. Res. Lett.,* **23,** 2971–2974.

Morrissey, M. L., and N. E. Graham, 1996: Recent trends in rain gauge precipitation measurements from the tropical Pacific: Evidence for an enhanced hydrologic cycle. *Bull. Amer. Meteor. Soc.,* **77,** 1207–1219.

Newell, R. E., and B. C. Weare, 1976: Ocean temperatures and large-scale atmospheric variations. *Nature,* **262,** 40–41.

Oort, A. H., 1983: Global atmospheric circulation statistics, 1958–1973. NOAA Prof. Paper 14, 180 pp.

Pan, Y. H., and A. H. Oort, 1990: Correlation analyses between sea surface temperature anomalies in the eastern equatorial Pacific and the world ocean. *Climate Dyn.,* **4,** 191–205.

Pierrehumbert, R. T., 1995: Thermostats, radiator fins, and the local runaway greenhouse. *J. Atmos. Sci.,* **52,** 1784–1806.

Rasmusson, E., and P. Arkin, 1993: A global view of large-scale precipitation variability. *J. Climate,* **6,** 1495–1521.

Ropelewski, C. F., and M. Halpert, 1987: Global and regional scale precipitation patterns associated with the El Niño/Southern Oscillation. *Mon. Wea. Rev.,* **115,** 1606–1626.

——, and ——, 1996: Quantifying Southern Oscillation–precipitation relationships. *J. Climate,* **9,** 1043–1059.

Smith, E. A., and Coauthors, 1998: Results of WETNET PIP-2 Project. *J. Atmos. Sci.,* **55,** 1483–1536.

Smith, T. M., and C. F. Ropelewski, 1997: Quantifying Southern Oscillation–precipitation relationships from an atmospheric GCM. *J. Climate,* **10,** 2277–2284.

Spencer, R. W., 1993: Global oceanic precipitation from the MSU during 1979–91 and comparisons to other climatologies. *J. Climate,* **6,** 1301–1326.

——, and J. R. Christy, 1990: Precise monitoring of global temperature trends from satellites. *Science,* **247,** 1558–1562.

——, F. J. LaFontaine, T. DeFelice, and F. J. Wentz, 1998: Tropical oceanic precipitation changes after the 1991 Pinatubo eruption. *J. Atmos. Sci.,* **55,** 1707–1713.

Sun, D. Z., and I. M. Held, 1996: A comparison of modeled and observed relationships between interannual variations of water vapor and temperature. *J. Climate,* **9,** 665–675.

Thomas, D., J. P. Duvel, and R. Kandel, 1995: Diurnal bias in calibration of broad-band radiance measurements from space. *IEEE Trans. Geosci. Remote Sens.,* **33,** 670–683.

Trenberth, K. E., 1998: Atmospheric moisture residence times and cycling: Implications for rainfall rates with climate change. *Climatic Change,* **39,** 667–694.

Weng, F., and N. C. Grody, 1994: Retrieval of cloud liquid water using the special sensor microwave imager. *J. Geophys. Res.,* **99,** 22 535–22 551.

Wentz, F. J., 1997: A well-calibrated ocean algorithm for SSM/I. *J. Geophys. Res.,* **102** (C4), 8703–8718.

——, and E. A. Francis, 1992: Nimbus-7 SMMR ocean products, 1979–1984. Remote Sensing Systems Tech. Rep. 033192, 36 pp. [Available from Remote Sensing Systems, 1101 College Ave., Santa Rosa, CA 95404.]

——, and R. W. Spencer, 1998: SSM/I rain retrievals within a unified all-weather ocean algorithm. *J. Atmos. Sci.,* **55,** 1613–1627.

Wetherald, R. T., V. Ramaswamy, and S. Manabe, 1991: A comparative study of the observations of high clouds and simulations by an atmospheric general circulation model. *Climate Dyn.,* **5,** 135–143.

Xie, P., and P. Arkin, 1997: Global precipitation: A 17-year monthly analysis based on gauge observations, satellite estimates, and numerical model outputs. *Bull. Amer. Meteor. Soc.,* **78,** 2539–2558.

Yulaeva, E., and J. M. Wallace, 1994: The signature of ENSO in global temperature and precipitation fields derived from the Microwave Sounding Unit. *J. Climate,* **7,** 1719–1736.